ARTICLE

Synthesis of $CuAl_2O_4$ & Fe substituted $CuAl_2O_4$ Nanospinels and CCD based Response Surface Methodology investigations for Pb^{2+} ions adsorption

Andal Gopal[1] **and R Lakshmipathy**[2,*]

[1] Department of Chemistry, KCG College of Technology, Chennai 600 097, India
[2] Directorate of Learning and Development, SRM Institute of Science and Technology, Katankullathur, Chengalpattu District, Tamil Nadu, India

Abstract

This study focuses on the synthesis of pure and Fe-substituted $CuAl_2O_4$ nanospinels using the co-precipitation method at elevated temperatures. Various analytical techniques, including scanning electron microscopy, transmission electron microscopy, FT-IR spectroscopy, and X-ray diffraction, were employed to confirm the formation of the nanospinels. The efficiency of the prepared nanospinels in adsorbing Pb^{2+} ions from aqueous solutions was evaluated. A Response Surface Methodology (RSM) based on a Central Composite Design (CCD) was developed to optimize three independent variables: pH, contact time, and initial concentration. A quadratic model was constructed to predict the adsorption behavior, and the model predictions closely matched the experimental values, indicating high reliability. The adsorption isotherm and kinetic studies suggest multilayer adsorption governed by the Langmuir isotherm, with physisorption as the dominant mechanism, although the kinetic data fitted well with the pseudo-second-order kinetic model. The spontaneity of the adsorption process increased with rising temperature and was found to be exothermic in nature. The adsorbents exhibited preferential uptake of Pb^{2+} ions, though the process was not selective. The adsorption mechanism of Pb^{2+} ions onto $CuAl_2O_4$ and $CuAlFeO_4$ nanospinels was elucidated as electrostatic attraction, which was confirmed by XPS analysis. The present work highlights the potential application of $CuAl_2O_4$ and $CuAlFeO_4$ nanospinels for the adsorption of Pb^{2+} ions.

Keywords: $CuAl_2O_4$; Adsorption; Lead; Nanomaterials; Co-precipitation

Citation
Andal Gopal and R Lakshmipathy (2026). Synthesis of $CuAl_2O_4$ & Fe substituted $CuAl_2O_4$ Nanospinels and CCD based Response Surface Methodology investigations for Pb^{2+} ions adsorption. Mari Papel Y Corrugado, 2026(1), 34–49.

1 Introduction

Spinel oxides have the general formula AB_2O_4, where cations A occupy one-eighth of the tetrahedral sites in a face-centered cubic (fcc) packed oxygen sublattice, and cations B occupy half of the octahedral sites. Spinel aluminates have attracted significant interest due to their applications in various fields such as catalysts, refractories, pigments, and sensors [1–4]. Copper aluminate is a promising material owing to its electronic, magnetic, optical, and catalytic properties and is widely applied in industries as coatings, pigments, and catalysts [5–7]. $CuAl_2O_4$ belongs to the inverse spinel structure, in which Cu^{2+} ions occupy one-eighth of the tetrahedral interstices, while Al^{3+} ions occupy half of the octahedral interstices [8].

Submitted: 3 February, 2026
Accepted: 4 March, 2026
Published: 4 April, 2026

Vol. 2026, **No.** 1, 2026.
https://doi.org/10.71442/mari2026-0004

***Corresponding author:**
✉ R Lakshmipathy
lakshmipathy.vit@gmail.com

Researchers have been drawn to $CuFe_2O_4$ because of its excellent magnetic characteristics; however, due to the weak interdiffusion of Cu^{2+} and Fe^{3+} ions, synthesizing $CuFe_2O_4$ remains a challenging task [9]. Studies on the effect of ion substitution in $CuAl_2O_4$ have not been extensively explored. To enhance the catalytic activity of $CuAl_2O_4$, several researchers have investigated Fe substitution in the material [10].

Magnetic substitution in $CuAlO_2$ has recently been investigated for thermoelectric applications. In such studies, transition metal ions such as Fe^{3+} are substituted for Al^{3+} ions. Some relevant literature reports are summarized below. Upon substituting Al^{3+} in $CuFe_2O_4$, a single-phase ferrite spinel is observed up to 950 °C; however, on further heating to 1050 °C and 1100 °C, the delafossite phase $CuFeO_2$ appears along with the primary ferrite spinel phase [11]. Trivedi et al. prepared Al^{3+}-substituted $CuFe_2O_4$, namely $CuAlFeO_4$, at 1000 °C for 24 h without any impurity phases [12]. Similarly, a pure $CuAlFeO_4$ compound was synthesized at 1200 °C for 20 h using the ceramic method [13]. Ata Allah synthesized $CuAlFeO_4$ by substituting Al^{3+} ions for Fe^{3+} ions in ferrite, which attracted considerable interest due to its non-magnetic nature [14]. In the present work, Fe^{3+} ions are substituted for Al^{3+} ions in $CuAl_2O_4$, as Fe^{3+} ions show a stronger preference for the B-site and are expected to impart magnetic properties. The introduction of magnetic Fe^{3+} ions into the octahedral sites of inverse spinel $CuAl_2O_4$ may result in interesting structural and magnetic characteristics. Accordingly, our objective is to synthesize copper aluminates doped with Fe ions at the B-site. Fe-substituted $CuAl_{2-x}Fe_xO_4$ (x = 0–1) samples were synthesized and systematically studied using X-ray diffraction

Ferrites and γ-Al_2O_3 have been explored well as an adsorbent for heavy metal ions [15, 16] Spinel ferrites have been used for adsorption of dyes, metal ions since it can be easily removed by magnetic means. Adsorption property of γ-Al_2O_3 are well reported. [17] reported in his work that Cu^{2+} ion in $CuAl_2O_4$ has found to be active centre for the adsorption of Nitrogen oxides. Nano Copper aluminates are applied in photo catalytic degradation of dyes due to its large surface area [18, 19] Even though $CuAl_2O_4$ has been explored well as a catalyst due to its adsorbent properties it is used for the removal of Cr(VI) ion [20].

Various methods have been employed for the synthesis of substituted spinel aluminates, including sol–gel [21], flame spray pyrolysis [22], co-precipitation [23], and ball milling [24]. The present work focuses on the synthesis of copper aluminates doped with Fe ions at the B-site. To the best of our knowledge, there are no literature reports on the use of $CuAl_2O_4$ and $CuAlFeO_4$ as adsorbents for the removal of heavy metal ions, particularly lead (Pb^{2+}). The primary objective of this study is to investigate the removal of the highly hazardous environmental pollutant lead using $CuAl_2O_4$ and $CuAlFeO_4$ as adsorbents. The adsorption properties of copper aluminates were examined with respect to Fe^{3+} substitution for Al^{3+}. In this work, the effect of Fe^{3+} substitution in $CuAl_2O_4$ was systematically studied using X-ray diffraction (XRD), Fourier-transform infrared spectroscopy (FTIR), scanning electron microscopy (SEM), transmission electron microscopy (TEM), and Brunauer–Emmett–Teller (BET) surface area analysis.

Lead is a toxic heavy metal with no known biological function. Its predominant oxidation state is +2, owing to the rare occurrence of Pb^0 and the extremely oxidizing conditions required for the formation of Pb^{4+}. The primary source of human exposure to lead is drinking water transported through corroded, lead-based plumbing materials. Various methods have been reported for the removal of lead from aqueous solutions, including precipitation, electrochemical treatment, liquid–liquid extraction, redox reactions, co-precipitation, adsorption, flocculation, reverse osmosis, ion exchange, and filtration [25]. However, most of these methods suffer from several drawbacks, such as high cost, low efficiency, limited applicability to a wide range of pollutants, and high time and chemical consumption [26]. The removal of heavy metal ions from aqueous media using simple and efficient techniques is therefore crucial in addressing water pollution. Among the available methods, adsorption is considered particularly effective for wastewater treatment due to its simplicity and efficiency [27]. Accordingly, in the present study, lead adsorption onto $CuAl_2O_4$ and Fe-substituted $CuAl_{2-x}Fe_xO_4$ (x = 1) nanospinels synthesized by the co-precipitation method was systematically investigated.

2 EXPERIMENTAL

2.1 Materials

Aluminium Nitrate (98%) and Alginic acid (19-25%) were procured from sd. fine-Chemical limited, India. Cuprous acetate (99%) from Sisco lab and NH_3 from Qualigens. Stock solution of 0.01M of Pb (II) was prepared from lead acetate using double distilled water. All the regents used were of analytical grade.

2.2 Preparation of $CuAl_2O_4$

Alginic acid solutions (5 wt%) were prepared using distilled water to obtain polymeric precursors. To improve solubility, a few drops of ammonia solution were added to the alginic acid. Cuprous acetate and aluminum nitrate solutions, each with a concentration of 1 M, were mixed in a 1:2 molar ratio and stirred to obtain a homogeneous solution. This metal ion solution was then slowly added to the 5 wt% alginic acid solution under continuous stirring, resulting in the formation of a copper–aluminum alginate precursor. The precursor was subsequently dried and calcined at different temperatures ranging from 100 to 900 °C, with each temperature maintained for six hours, to obtain pure $CuAl_2O_4$.

2.3 Preparation of $CuAlFeO_4$

Equimolar (1 M) solutions of cuprous acetate, aluminum nitrate, and ferric nitrate were mixed in equal volumes and stirred to obtain a homogeneous solution. This metal ion solution was then gradually added to the 5 wt% alginic acid solution under continuous stirring, leading to the formation of a copper–aluminum–iron alginate precursor. The precursor was subsequently dried at 100 °C and then calcined at temperatures up to 800 °C for 12 h. After calcination, the resulting powder was compacted into pellets and sintered at 900 °C for 12 h. Finally, the samples were allowed to cool slowly to room temperature, yielding pure $CuAlFeO_4$.

2.4 Characterization

The phases present in the as-synthesized powders (A and B) were characterized by powder X-ray diffraction (XRD) at room temperature using a Bruker D8 Advance diffractometer with Cu Kα radiation (λ = 1.54 Å). The average crystallite size of the synthesized products was estimated using the Debye–Scherrer equation. Fourier-transform infrared (FTIR) spectra were recorded using a JASCO Model 4100 spectrometer with the KBr pellet technique. Scanning electron microscopy (SEM) analysis was performed using an FEI QUANTA FEG 200 HR scanning electron microscope. Transmission electron microscopy (TEM) images were obtained using a Philips CM 200 instrument operated at an accelerating voltage of 20–200 kV. The residual Pb(II) concentration in solution was determined using an atomic absorption spectrophotometer (Varian AA 240). The specific surface areas of the samples were measured by nitrogen adsorption isotherms using an ASAP-2020 (V3.00 H) surface area analyzer.

2.5 Adsorption investigations

All the adsorption studies were carried out in the 100 ml glass beakers. The working volume of the Pb^{2+} solution was taken as 25 ml and crucial variables such as pH, contact time and initial concentration was fixed according to the Central Composite Design (CCD) of Response Surface Methodology (RSM) and adsorbent dose was fixed as 0.025 g for all the 20 runs. Immediately after the addition of the adsorbents ($CuAl_2O_4$ and $CuAlFeO_4$), the solutions were stirred in a magnetic stirrer at 170 rpm for the adsorption of Pb^{2+} ions on to the adsorbents. The experiment was conducted in room temperature (29°C). After completion of the experiments, the suspension was filtered through Whatman No 1001-125 (dia125 mm) filter paper. The concentration of Pb^{2+} ions present in the filtrate was determined by Atomic Absorption Spectrophotometer (AAS) and the quantity and percentage of Pb^{2+} ions adsorbed was calculated using the below equations.

$$\% R = \frac{C_0 - C_1}{C_0} x\ 100 \quad (1)$$

$$Loading\ capacity\ (q_e) = \frac{C_0 - C_1}{m} V \quad (2)$$

Where C_o is the initial concentration of the Pb^{2+} ions and C_1 is the final or residual concentration. V is the volume and m is the mass of the $CuAl_2O_4$ and $CuAlFeO_4$ adsorbents

2.6 Response Surface Methodology

Central Composite Design (CCD) was developed using Response Surface Methodology for the

optimization of three independent variables such as pH, contact time and adsorbent dose for the removal of lead ions from aqueous solution. The values selected for the variables were done based on the preliminary experimental results. A Design expert version 13.0 software was used for the development of CCD and optimization of the multivariate. The CCD has a total of 20 runs containing 6 axial, 6 center and 8 factorial points to determine the optimal conditions. The coded variables for the relationship between the removal of lead ions and independent variables in the form of polynomial quadratic model are presented in equation 3 for $CuAl_2O_4$ and in equation 4 for $CuAlFeO_4$:

$$\%\ Removal = 98.58 + 1.57\ A + 14.49\ B - 4.82\ C - 24.31\ A^2 - 8.09\ B^2 - 2.27\ C^2 + 0.750\ AB - 1.25\ AC + 2.00\ BC \quad (3)$$

$$\%\ Removal = 98.62 + 1.19\ A + 14.37\ B - 4.84\ C - 24.58\ A^2 - 8.03\ B^2 - 2.18\ C^2 + 1.000\ AB - 1.25\ AC + 2.00\ BC \quad (4)$$

Where A is the pH, B is contact time and C is the initial concentration and the selected summary of levels is represented in Table 1.

Table 1. Optimization of independent variables, their levels and symbols

Variables	Symbol	Levels		
		-1	0	+1
pH	A	4	6	8
Contact time	B	30	75	120
Initial Concentration	C	30	45	60

3 Results and Discussion

3.1 Characterisation of adsorbent

Figure 1 shows the X-ray diffraction (XRD) pattern of the $CuAl_2O_4$ precursor calcined at 900 °C for 6 h, while Figure 2 presents the compiled XRD patterns of the $CuAlFeO_4$ precursor heated at different temperatures for 12 h. CuO peaks are observed along with $CuAl_2O_4$ peaks up to 700 °C. The formation of pure $CuAlFeO_4$ is observed at 900 °C. All the diffraction peaks can be indexed to the cubic spinel structure of $CuAl_2O_4$ (JCPDS file No. 78-1605) [28]. Based on the powder XRD data, the crystallite sizes of the as-prepared powders were calculated using the Scherrer equation.

$$D = \frac{K\lambda}{\beta\cos\theta} \quad (5)$$

Where β is the full width maximum, K is shape factor (0.9) and λ is the wavelength of X-ray source. The grain size calculated for $CuAl_2O_4$and $CuAl_{2-x}Fe_xO_4$ is given in Table.2. In order to understand the influence of Fe substitution in 'B' site of $CuAl_2O_4$, lattice Constant is calculated. It is observed that the lattice constant of $CuAl_2O_4$ increases with Fe substitution which is given in Table1. Increase in lattice constant 'a' on substitution of Fe is due to the fact that the Pauling ionic radius of Fe^{3+} (0.64Å) is greater than that of Al^{3+} (0.51Å). The grain size calculated for $CuAl_2O_4$ (9.71nm) decreases on Fe substitution in $CuFeAlO_4$ (8.75nm).

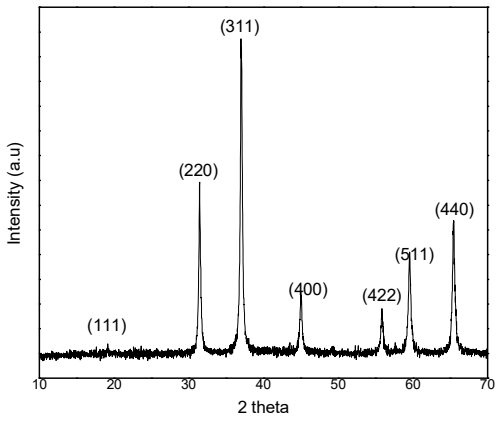

Figure 1. Powder XRD pattern of CuAl2O4 nanospinel

Table 2. Lattice parameter, density, Volume and particle size of $CuAl_2O_4$ and $CuFeAlO_4$ nanospinels

Sample	Lattice Parameter (Å)	Density (g/cm^3)	Volume ($Å^3$)	Particle size (nm)
$CuAl_2O_4$	8.05	4.62	522	9.7
$CuFeAlO_4$	8.25	5.08	563	8.7

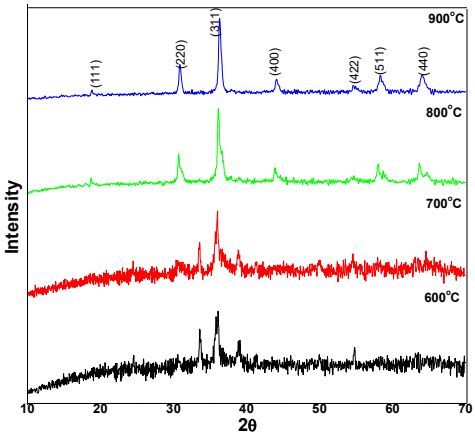

Figure 2. Powder XRD pattern of $CuAl_{2-x}Fe_xO_4$ nanospinels synthesised at various temperatures

The FTIR pattern of $CuAl_2O_4$ (Fig.3.a) shows the characteristic peak of Al-O and Cu-O-Al-O at 595 cm^{-1}. The absorption band on Fe substitution becomes narrow at 615 cm^{-1} (Fig.3b) [28]. The SEM images of $CuAl_2O_4$ are given in Fig.4.a. The particles of nano size are found to be agglomerated. SEM image of $CuAlFeO_4$ (Fig.4.b) shows the formation of well-defined particles with almost uniform shape. Due to the absence of any stabilizing agent the particles are found to be agglomerated. EDX analysis of $CuAlFeO_4$ (Fig.5) confirms the presence of Fe in $CuAl_2O_4$.

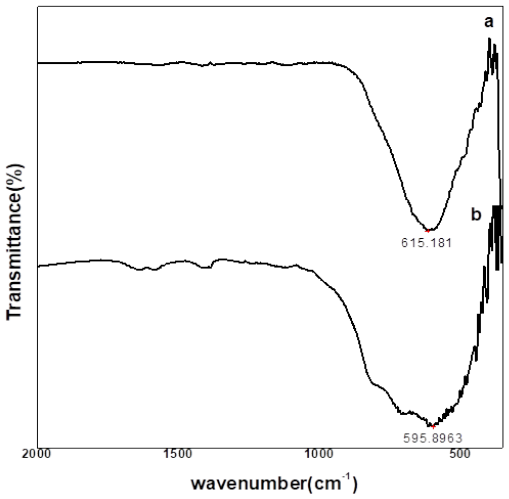

Figure 3. FTIR pattern of a) $CuAl_2O_4$ b) $CuAl_{2-x}Fe_xO_4$ nanospinels synthesised in this study

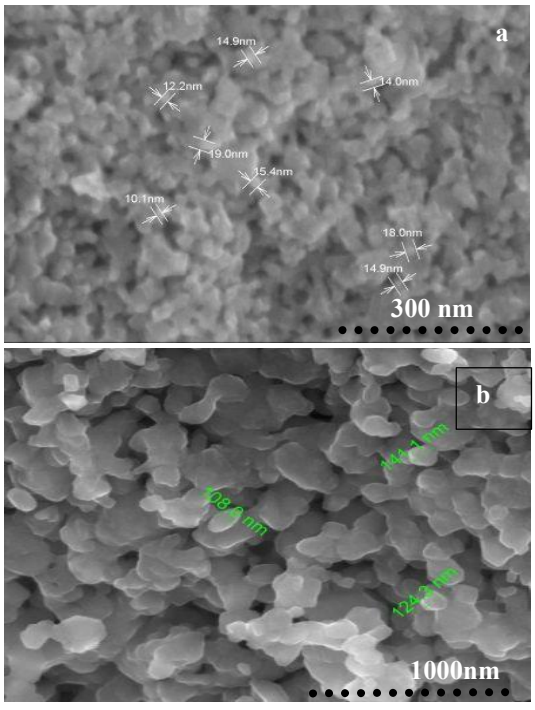

Figure 4. SEM images of a) $CuAl_2O_4$ b) $CuAl_{2-x}Fe_xO_4$ nanospinels synthesised in this study

Examination of the TEM image of $CuAl_{2-x}Fe_xO_4$ confirms the formation of rectangular shape nano particles (Fig.6). The surface area values determined by BET-N_2 surface area method for $CuAl_2O_4$ and $CuAlFeO_4$ are 23.1 and 23.9 m^2/g respectively.

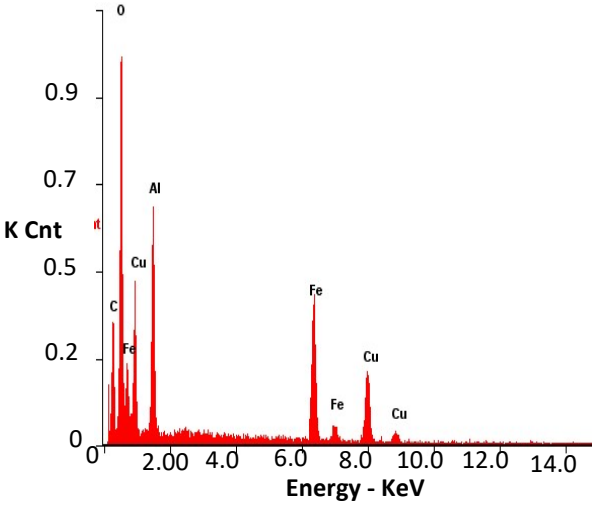

Figure 5. EDAX pattern of $CuAl_{2-x}Fe_xO_4$ nanospinels synthesised in this study

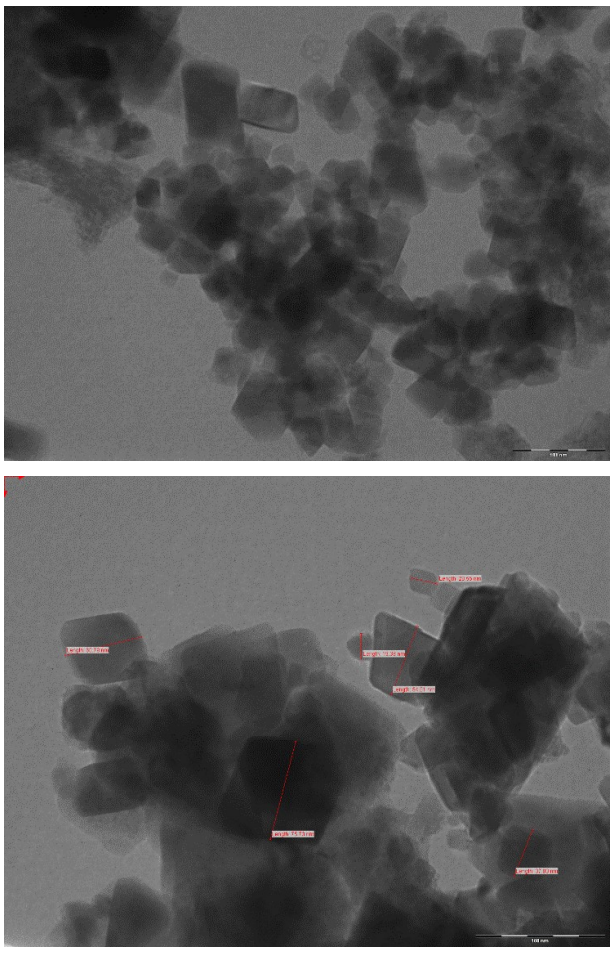

Figure 6. TEM images of $CuAlFeO_4$ nanospinels synthesised in this study

3.2 Response surface methodology

The reliability of the models can be verified based on number of factors that can be derived from the output of the data. In this study, the Central Composite Design (CCD) was developed for the removal of Pb^{2+} ions by $CuAl_2O_4$ and $CuAlFeO_4$ nanomaterials from aqueous solution. Three independent variables that are imperative for adsorption of Pb^{2+} ions are optimised by the CCD and the results of the 20 runs are summarised in Table-3. The percentage removal of Pb^{2+} ions by $CuAl_2O_4$ and $CuAlFeO_4$ nanomaterials were found to be high at pH 6 for an initial concentration of 45 mg L^{-1} with a contact time of 75 min. The experimental removal efficiencies calculated for all runs are very close to the predicted values of the model suggesting the high reliability and applicability of the developed model.

Table 3. Experimental and predicted design matrix factors of CCD for the removal of Pb^{2+} ions by $CuAl_2O_4$ and $CuAlFeO_4$ nanospinels

Run no.	pH	Contact time (min)	Initial Concentration (mg/L)	% Removal			
				$CuAl_2O_4$		$CuAlFeO_4$	
				Exp.	Pre.	Exp.	Pre.
1	6	75	45	99.6	98.5	99.7	98.6
2	6	10	45	55.2	60.7	56.5	61.1
3	9.3	75	45	31.5	34.9	29.9	33.6
4	6	75	45	99.5	98.5	99.6	98.6
5	6	75	45	99.6	98.5	99.6	98.6
6	8	30	30	61.0	58.3	60.8	57.7
7	6	75	45	99.4	98.5	99.8	98.6
8	6	75	45	99.7	98.5	99.4	98.6
9	8	120	60	79.1	76.6	78.4	76.2
10	4	30	60	46.3	43.0	45.8	43.6
11	4	120	60	75.3	74.5	75.9	74.4
12	6	75	45	99.5	98.5	99.4	98.6
13	4	120	30	77.7	77.6	76.8	77.5
14	4	30	30	55.9	54.1	56.6	54.8
15	6	75	70	80.3	84.2	81.5	84.4
16	8	120	30	85.2	84.7	86.6	84.4
17	6	150	45	100	100	100	100
18	8	30	60	46.3	42.1	46.8	41.5
19	2.6	75	45	25.3	25.6	26.4	25.5
20	6	75	20	100	100	100	100

Statistical analysis of the present model developed for the removal of Pb^{2+} ions by $CuAl_2O_4$ and $CuAlFeO_4$ nanomaterials was performed using the Design Expert software 13.0 and the data is represented in Table 4 & 5. The probability value (p-value) that defines the significance of the model was found to be < 0.0001 for the removal of Pb^{2+} ions by $CuAl_2O_4$ and $CuAlFeO_4$ nanomaterials as seen in Table 4 & 5. A p-value of < 0.0001 indicates that the present model is significant for both the adsorbents and suggesting that the results are significant and reliable. The F-values of the both the models were found to be 123.7 and 136.8 respectively towards $CuAl_2O_4$ and $CuAlFeO_4$ nanomaterials. F-values this high in this study indicates that the model is significant and better fits and the high values also suggest that only 0.01% of chance to occur due to noise [29,30].

Table 4. ANOVA data and values for the removal of Pb^{2+} ions by $CuAl_2O_4$ nanospinels

Source	Sum of Squares	df	Mean Square	F-value	p-value
Model	11854.48	9	1317.16	123.71	< 0.0001
A-pH	33.45	1	33.45	3.14	0.1067
B-Contact Time	2661.49	1	2661.49	249.97	< 0.0001
C-Initial Concentration	314.89	1	314.89	29.57	0.0003
AB	4.50	1	4.50	0.4226	0.5303
AC	12.50	1	12.50	1.17	0.3040
BC	32.00	1	32.00	3.01	0.1137
A^2	8468.02	1	8468.02	795.31	< 0.0001
B^2	756.50	1	756.50	71.05	< 0.0001
C^2	72.31	1	72.31	6.79	0.0262
Residual	106.47	10	10.65		
Lack of Fit	106.47	5	21.29		
Pure Error	0.0000	5	0.0000		
Cor Total	11960.95	19			
Std. Dev	3.26				
R^2	0.9911				
Adjusted R^2	0.9831				
Predicted R^2	0.9386				
Press	734.7				
Adequate precision	32.36				

The correlation coefficients obtained in this study for both the models are closer to one and the reliability of the model is further propounded by the adjusted and predicted R^2 values that are closer to

the actual R^2 values. The closer correlation values of adjusted and predicted suggest that the correlation is high and desirable. The signal to noise ratio can be determined by the adequate precision and any values > 4 is desirable and in this study, the adequate precision is found to be 32.36 and 33.98. These high adequate precision values suggest that the model provide adequate signals and desirable. Further smaller standard deviation values of 3.26 and 3.12 propound that the developed models have excellent precision of the regression equation. The diagnostic plots of experimental and predicted values are presented in Fig. 7 and the points of distribution lay straight in the line suggesting that no significant deviation took place and bolsters the regression model [31].

Table 5. ANOVA data and values for the removal of Pb^{2+} ions by $CuAlFeO_4$

Source	Sum of Squares	df	Mean Square	F-value	p-value
Model	11977.22	9	1330.80	136.38	< 0.0001
A-pH	19.35	1	19.35	1.98	0.1894
B-Contact Time	2617.17	1	2617.17	268.20	< 0.0001
C-Initial Concentration	318.11	1	318.11	32.60	0.0002
AB	8.00	1	8.00	0.8198	0.3865
AC	12.50	1	12.50	1.28	0.2841
BC	32.00	1	32.00	3.28	0.1003
A^2	8655.82	1	8655.82	887.01	< 0.0001
B^2	744.24	1	744.24	76.27	< 0.0001
C^2	67.17	1	67.17	6.88	0.0254
Residual	97.58	10	9.76		
Lack of Fit	97.58	5	19.52		
Pure Error	0.0000	5	0.0000		
Cor Total	12074.80	19			
Std. Dev	3.12				
R^2	0.9919				
Adjusted R^2	0.9846				
Predicted R^2	0.9431				
Press	686.6				
Adequate Precision	33.98				

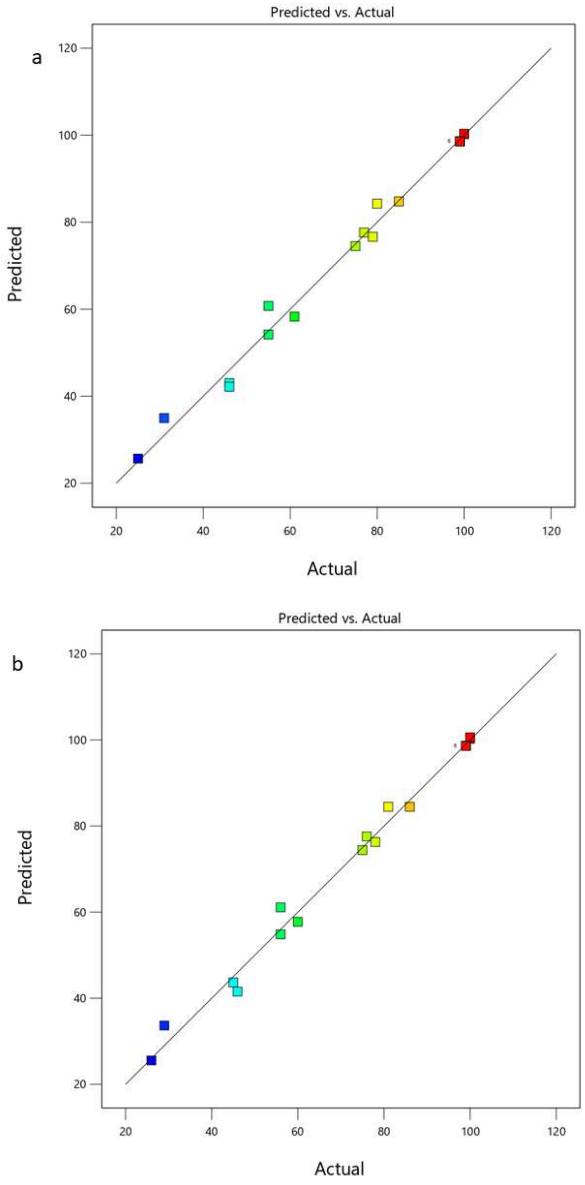

Figure 7. Actual and Predicted values correlation for the removal of Pb^{2+} ion by a) $CuAl_2O_4$ and b) $CuAlFeO_4$ nanospinels

The interaction among the selected independent variables can be graphically visualised in order to better understand how each variables influence each other for the removal of Pb^{2+} ions by the $CuAl_2O_4$ and $CuAlFeO_4$ nanomaterials. The 3D and contour plots of interaction of independent variables towards removal of Pb^{2+} by $CuAl_2O_4$ and $CuAlFeO_4$ nanomaterials are shown in Fig. 8 & 9. The interactions among pH and contact time suggest that the removal efficiencies are high at pH 6 and at longer contact time intervals typically above 75 min Fig 8a & 9a. In the case of pH, increase or decrease in the pH results in reduced removal efficiency for both nanoadsorbents. The optimal removal efficiency achieved at pH 6 is attributed to the point

zero charge (pH_{pzc}) of the $CuAl_2O_4$ and $CuAlFeO_4$ nanomaterials and the pH_{pzc} were found to be 5.9 and 6.0 respectively for $CuAl_2O_4$ and $CuAlFeO_4$ nanomaterials. The interaction 3D and contour plots of pH and initial concentration recommends that optimal removal efficiencies are observed at lower initial concentrations at pH 6 and with surge in initial concentration the removal efficiencies tend to decline and this trend is observed due to exhaustion of the active sites on the surface of the adsorbents (Fig. 8b & 9b). These observations put forward that the efficiency of removal is maximum at lower concentrations typically less than 50 mg L^{-1}. In the case of contact time and initial concentrations, the maximum removal efficiency is subject to higher contact time with lower initial concentrations. The 3D and contour plots (Fig. 8c & 9c) of initial concentration and contact time propounds that the removal of Pb^{2+} ions by $CuAl_2O_4$ and $CuAlFeO_4$ nanomaterials is maximum at 75 min of contact time with an initial concentration of 45 mg L^{-1}. The 3D plots obtained for all the independent variables interaction of $CuAl_2O_4$ and $CuAlFeO_4$ nanomaterials are found to be similar suggesting that both the nanomaterials have same nature and tendency to uptake the Pb^{2+} ions

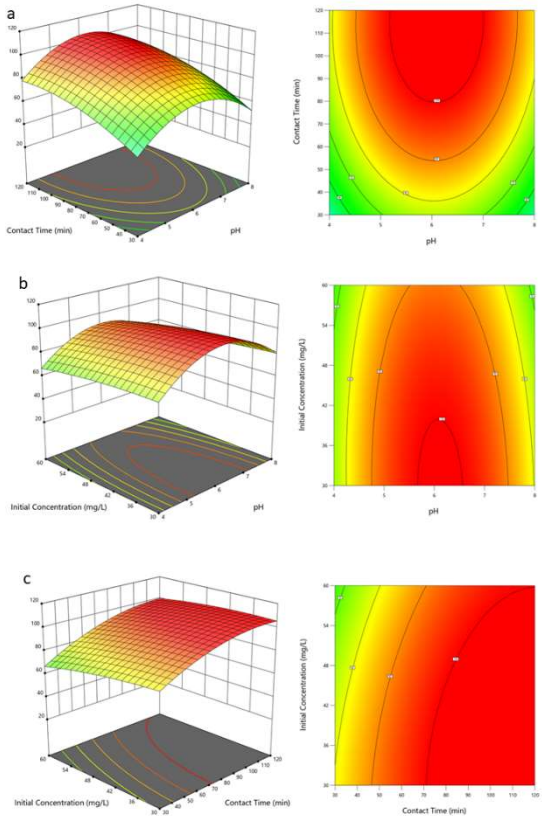

Figure 8. 3D surface and Contour plots for the removal of Pb^{2+} ions by $CuAl_2O_4$ nanospinels

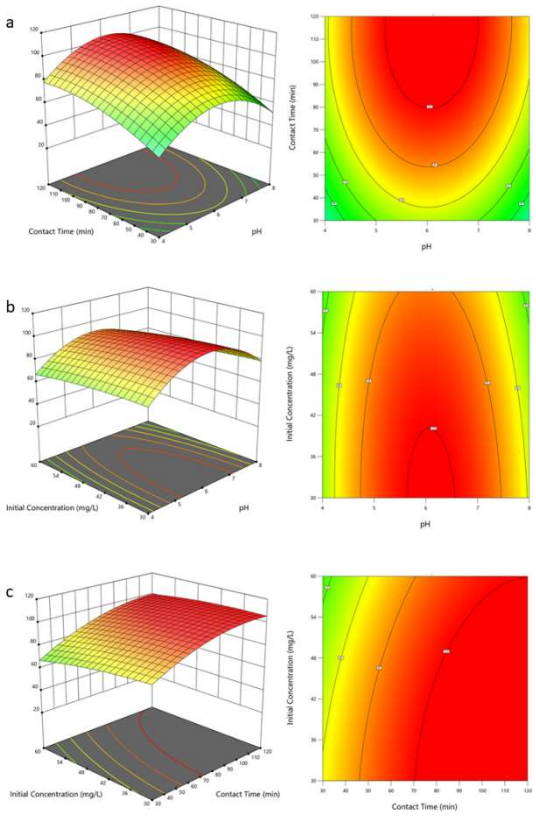

Figure 9. 3D surface and Contour plots for the removal of Pb^{2+} ions by $CuAlFeO_4$ nanospinels

3.2.1 *Adsorption isotherms*

The mathematical models such as isotherms are very much helpful in understanding the process of adsorption of Pb^{2+} ion onto the adsorbent such as nanomaterials. In order to predict and understand the process of the adsorption of Pb^{2+} ions onto $CuAl_2O_4$ and $CuAlFeO_4$, two well-known isotherm models such as Langmuir and Freundlich models were adopted and analysed the experimental data. The plots of isotherm models and their respective correlation coefficients are represented in Fig. 10 & 11 and Table 6.

The results of the Langmuir and Freundlich isotherms provided useful observations on the removal of Pb^{2+} ions by the $CuAl_2O_4$ and $CuAlFeO_4$ adsorbents. The equilibrium data tend to fit well with the Langmuir and Freundlich isotherms as seen in the Fig. 10 & 11. The correlation coefficients of Langmuir are observed to be close to one compared to be Freundlich isotherm however the correlation coefficients of Freundlich are acceptable. The applicability of Langmuir is further reinforced with the experimental loading capacities coinciding with theoretical values. These observations

propound that the Pb^{2+} ions adsorption onto $CuAl_2O_4$ and $CuAlFeO_4$ follow multilayer adsorption and each layer obeys Langmuir isotherm. Several studies have reported similar observations [32,33].

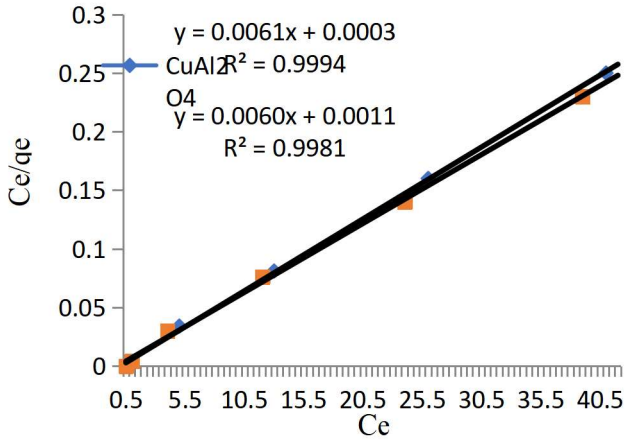

Figure 10. Langmuir plots for the removal of Pb^{2+} ions by $CuAl_2O_4$ and $CuAlFeO_4$ nanospinels

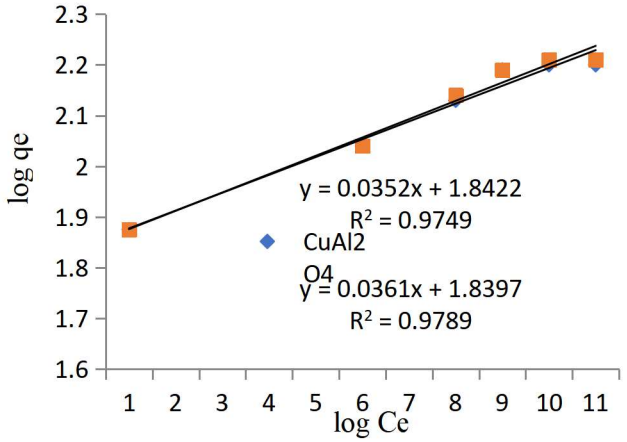

Figure 11. Freundlich plots for the removal of Pb^{2+} ions by $CuAl_2O_4$ and $CuAlFeO_4$ nanospinels

Table 6. Correlation coefficients and parameter values of isotherms

Model	Equation	Parameters	$CuAl_2O_4$	$CuAlFeO_4$
Freundlich	$logq_{e=}logK_f + \frac{1}{n}logC_e$	K_f	1.84	1.83
		1/n	0.0352	0.0361
		R^2	0.974	0.978
Langmuir	$\frac{C_e}{q_e} = \frac{1}{bV_m} + \frac{C_e}{V_m}$	b	0.0003	0.0011
		V_m	163.9	166.6
		R^2	0.999	0.998

3.2.2 *Kinetics of adsorption*

The rate of adsorption is very essential to understand and predict the mechanism of adsorption of adsorbate onto adsorbent surface and in view of that the kinetic data obtained for the removal of Pb^{2+} ions by $CuAl_2O_4$ and $CuAlFeO_4$ were analysed with various kinetic models. Further to elucidate the mechanism, investigations were performed by varying the temperature and rate constants were determined. The plots and kinetic constants obtained are summarised and presented in Fig. 12 & 13 and Table 7 & 8.

The outcomes of the kinetic models, namely pseudo-first-order (PFO) and pseudo-second-order (PSO), offer intriguing insights. Both models demonstrate a good fit with the kinetic data, resulting in linear plots with high correlation coefficients across all study temperatures. The correlation coefficients obtained for PFO and PSO at various temperatures in this investigation were consistently close to one. However, when examining the q_t values, it becomes evident that PSO values closely align with the experimental values compared to PFO (Fig. 12a&b). These findings suggest that PSO provides a more accurate representation of the kinetic data, with correlation coefficients and q_t values closely matching theoretical values (Fig.12 c&d).

The implication is that if PSO is applicable, the rate-limiting step should involve chemical reactions, specifically those encompassing the transfer of electrons leading to chemisorption [34]. To confidently assert that the removal of Pb^{2+} ions by $CuAl_2O_4$ and $CuAlFeO_4$ is governed by chemical reactions, several conditions must be met, as follows [35]:

(1) The rate constant remains unchanged at all initial concentrations of the adsorbate

(2) The rate constant remains unchanged irrespective of the agitation speed and

(3) The rate constant remains unchanged on all varying particle size of the adsorbents

To ascertain the validity of the specified conditions and confirm that chemisorption serves as the limiting factor in this investigation, assessments were carried out by manipulating the initial concentration of Pb^{2+} ions. Kinetic experiments were executed at initial Pb^{2+} ion concentrations of 45 and 60 mg L^{-1}, and the findings are outlined in Tables 7 and 8. It was observed that the rate constants (k_2) were not consistent and displayed variability in response to changes in initial concentrations. In cases where chemical reactions are the rate-

determining step, altering the initial concentration should not influence the reaction rate, and it should remain constant. The observed variation in rate constants indicates that chemical reactions and chemisorption, despite demonstrating a better fit to PSO, do not govern the rate-limiting step.

Moreover, the PSO equation is elaborated further through its representation as the Arrhenius equation with temperature as a variable. This expression offers insights into the nature of adsorption. The activation energy, derived from the Arrhenius equation, serves as an indicator of the type of adsorption of Pb^{2+} ions onto $CuAl_2O_4$ and $CuAlFeO_4$. Plots of $\ln k_2$ against 1/T resulted in linear relationships, and the activation energy (E_a) was determined from the slope. For $CuAl_2O_4$, activation energies of 3.78 and 4.15 kJ mol^{-1} were calculated for initial Pb^{2+} ion concentrations of 45 and 60 mg L^{-1}, respectively. Similarly, for $CuAlFeO_4$, activation energies of 5.47 and 3.90 kJ mol^{-1} were determined for the corresponding initial concentrations. Activation energies below 8.0 kJ mol^{-1} suggest a preference for physio-sorption over chemisorption, as the latter typically requires higher activation energies (around 40 kJ mol^{-1}) [36]. The positive E_a values suggest that adsorption is favourable at elevated temperatures, and pore diffusion is deemed suitable for the absorption of Pb^{2+} ions by both adsorbents.

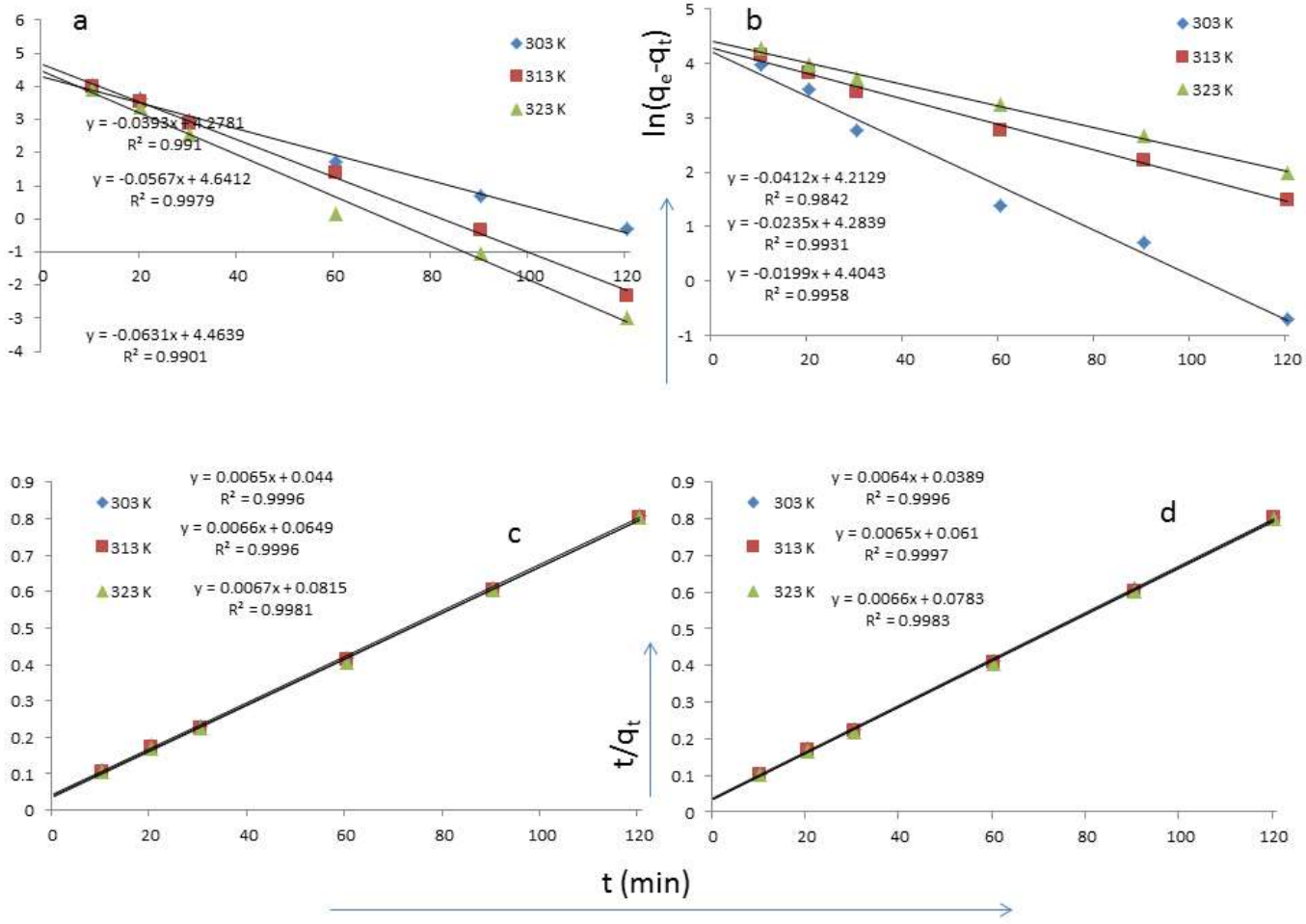

Figure 12. Kinetic plots of a) PFO of $CuAl_2O_4$ b) PFO of $CuAlFeO_4$ c) PSO of $CuAl_2O_4$ and d) PSO of $CuAlFeO_4$ at initial concentration 60 mg L^{-1}.

Advancing in the study, the kinetic data underwent analysis and was fit to the intra-particle diffusion model. The resulting plots of q_t against $t^{1/2}$ are depicted in Fig 13, offering valuable insights into the adsorption of Pb^{2+} ions onto the surfaces of $CuAl_2O_4$ and $CuAlFeO_4$ adsorbents. At lower temperatures (303 K), the adsorption process onto $CuAl_2O_4$ unfolds as a two-step mechanism. The initial step, or zone, is characterized by the rapid utilization of surface sites, followed by a slower diffusion into the

inner pores observed in the second zone. As the temperature increases, the adsorption capacity increases while the trend remains the same. Similar trends were noticed for the plots of Pb^{2+} ions removal by $CuAlFeO_4$ nanoadsorbent at various temperatures. These observations suggest that the adsorption of Pb^{2+} ions is favoured at elevated temperatures on both $CuAl_2O_4$ and $CuAlFeO_4$ adsorbents.

Table 7. Kinetic parameters for the removal of Pb^{2+} by $CuAl_2O_4$ nanomaterials

Model	Parameters	303 K		313 K		323 K	
		45	60	45	60	45	60
Pseudo first order	k_1	0.031	0.039	0.019	0.022	0.016	0.018
	q_e	21.7	28.9	21.9	29.1	22.6	29.8
	R^2	0.990	0.991	0.992	0.997	0.996	0.990
Pseudo second order	k_2	0.023	0.021	0.022	0.020	0.021	0.019
	q_e	110.9	153.8	111.6	154.5	112.4	155.2
	R^2	0.999	0.999	0.998	0.999	0.999	0.998

Table 8. Kinetic parameters for the removal of Pb^{2+} by $CuAlFeO_4$ nanomaterials

Model	Parameters	303 K		313 K		323 K	
		45	60	45	60	45	60
Pseudo first order	k_1	0.037	0.041	0.020	0.023	0.018	0.019
	q_e	23.8	31.3	24.1	31.6	24.7	32.4
	R^2	0.990	0.984	0.996	0.993	0.997	0.995
Pseudo second order	k_2	0.024	0.022	0.022	0.021	0.021	0.020
	q_e	111.7	156.2	112.5	156.8	113.1	157.5
	R^2	0.999	0.999	0.998	0.999	0.999	0.998

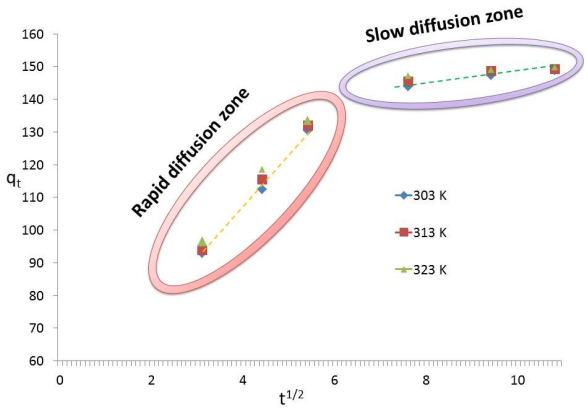

Figure 13. Weber and Morris intra-particle diffusion plots for the removal of Pb^{2+} ions by $CuAl_2O_4$ nanospinels

3.2.3 *Thermodynamics of adsorption*

The data sourced from change in temperature investigations can be prolifically used to understand the nature of the Pb^{2+} ions adsorption onto the $CuAl_2O_4$ and $CuAlFeO_4$ adsorbents. It is noticed that with the rise in temperature, the loading capacity and removal efficiency improved. The improved efficiencies or loading capacities at higher temperature is due to greater diffusion of Pb^{2+} ions into the inner pores of the materials. The thermodynamic parameters which are generally used to evaluate the adsorption process were derived using the below equation and their values are summarized in Table-9.

$$K_D = \frac{q_e}{C_e} \quad (6)$$

$$\Delta G^\circ = -RT\, lnK_D \quad (7)$$

$$\Delta G^\circ = \Delta H^\circ - T\Delta S^\circ \quad (8)$$

$$lnK_D = \frac{\Delta S^\circ}{R} - \frac{\Delta H^\circ}{RT} \quad (9)$$

"Where K_D is the equilibrium constant, R is gas constant and T is temperature"

Table 9. Thermodynamic parameter values for the removal of Pb^{2+} ions by $CuAl_2O_4$ and $CuAlFeO_4$ nanospinels

Adsorbent	Temperature (K)	Loading capacity q_e (mg g^{-1})	Free energy (ΔG°)	Enthalpy (ΔH°)	Entropy (ΔS°)
$CuAl_2O_4$	303	144.0	-10314	-8762	1443
	313	145.5	-11430		
	323	147.3	-13200		
$CuFeAlO_4$	303	145.5	-11065	-9230	1737
	313	147.0	-12512		
	323	148.3	-14540		

The results of the thermodynamic parameters propound that the present process of removal of Pb^{2+} ions by $CuAl_2O_4$ and $CuAlFeO_4$ nanospinels is spontaneous at all investigated temperatures and the spontaneity increases with rise in temperature which is evidenced by the higher negative change in free energy (ΔG°) values. In the case of $CuAlFeO_4$, the spontaneity is higher than the $CuAl_2O_4$ which is also noticed from the ΔG° values. The negative enthalpy (ΔH°) values indicate that the process of Pb^{2+} ions removal is exothermic in nature and high negative values suggest that it is highly exothermic in nature. The positive entropy (ΔS°) values indicate that the randomness increases with release of heat during adsorption [37].

3.2.4 *Regeneration and reuse*

The merits of the adsorbents are usually assessed on the capability of regenerative ability and their reuse in order to make it more economical. In view of the above, regeneration of the spent $CuAl_2O_4$ and $CuAlFeO_4$ nanospinels were performed using selective desorbing agents such as acids and bases. The results of the regeneration efficiencies of various desorbing agents are represented in Fig. 14. It is observed that the regeneration of the nanospinels were almost 100 % for HCl followed by CH_3COOH with regeneration efficiencies around 80 %. The bases exhibited poor regeneration efficiencies compared to acids and the superior regeneration efficiency exhibited by the acids are due to competition between hydronium ions and Pb^{2+} ions thus dislodging them from the surface. The 99 % regeneration efficiency exhibited by the nanospinels suggests that the adsorption of Pb^{2+} ions onto $CuAl_2O_4$ and $CuAlFeO_4$ is physio-sorption due to ion exchange nature. The regenerated nanospinels were reused to assess their reusability for 3 cycles and the efficiency remains almost close to the 1st cycle of adsorption of Pb^{2+} ions. The established regeneration and reusability abilities of the $CuAl_2O_4$ and $CuAlFeO_4$ nanospinels make it more attractive choice of adsorbents for the real time wastewater treatment.

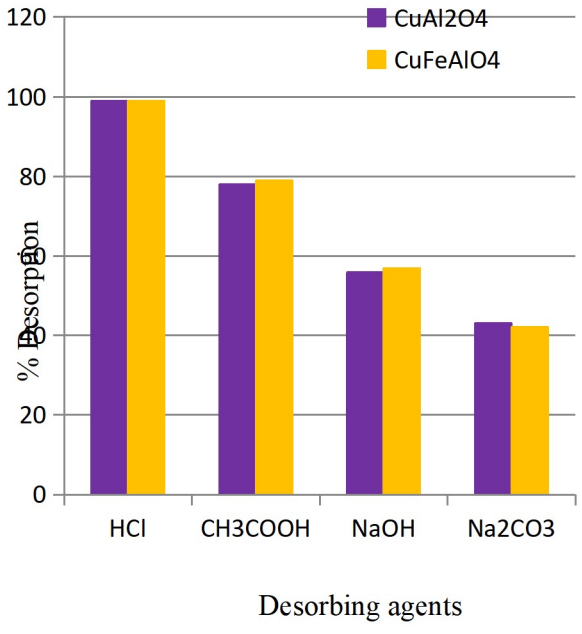

Figure 14. Regeneration of $CuAl_2O_4$ and $CuAlFeO_4$ nanospinels by various desorbing agents

3.2.5 *Selectivity and loading capacities*

Since the real time samples might contains varying concentrations of various metal ions, it is highly essential to investigate the selective adsorption ability of the adsorbents. Investigations were performed to understand if the $CuAl_2O_4$ and $CuAlFeO_4$ nanospinels have selectivity towards Pb^{2+} ions from mixture of metal ions. A mixture of 50 ml of multi metal solution containing Pb^{2+}, Cd^{2+}, Co^{2+}, Ni^{2+} and Zn^{2+} ions with each metal concentration being 50 mg L^{-1} was prepared and tested for their removal against $CuAl_2O_4$ and $CuAlFeO_4$ nanospinels. The results of the investigations are summarised and presented in Table-10. It is clearly evident that the $CuAl_2O_4$ and $CuAlFeO_4$ nanospinels have preferential uptake towards Pb^{2+} ions compared to other co-metal ions that were selected in this study. The removal efficiency towards Pb^{2+} ions by both the nanospinels were above 85 % and exhibited higher loading capacities as well. The Cd^{2+} ions were also moderately adsorbed by the $CuAl_2O_4$ and $CuAlFeO_4$ nanospinels in addition to Pb^{2+} ions. The adsorption of Co^{2+}, Ni^{2+} and Zn^{2+} was very poorly removed by the $CuAl_2O_4$ and $CuAlFeO_4$ nanospinels. The preferential uptake of Pb^{2+} ions is due to smaller ionic radius compared to other co-cations that can easily get accommodated in the inner pores of the $CuAl_2O_4$ and $CuAlFeO_4$ nanospinels [38]. These observations propounds that $CuAl_2O_4$ and $CuAlFeO_4$ nanospinels have preferential uptake of Pb^{2+} ions but not selective towards Pb^{2+} ions. To further establish the merits of the $CuAl_2O_4$ and $CuAlFeO_4$ nanospinels a comparison of loading capacities of various nanoadsorbents towards Pb^{2+} ions are summarised in Table-11. It is worth noting that the loading capacities of $CuAl_2O_4$ and $CuAlFeO_4$ nanospinels are higher than several nanoadsorbents reported in literature.

Table 10. Multi-metal removal results of $CuAl_2O_4$ and $CuAlFeO_4$ nanospinels

Metal ion	% Removal		Loading capacity (mg g^{-1})	
	$CuAl_2O_4$	$CuFeAlO_4$	$CuAl_2O_4$	$CuFeAlO_4$
Pb^{2+}	86.7	87.1	108.3	108.8
Cd^{2+}	52.3	51.9	65.3	64.8
Co^{2+}	9.4	9.6	11.7	12.0
Ni^{2+}	11.8	11.6	14.7	14.5
Zn^{2+}	6.5	6.2	8.1	7.7

Table 11. Loading capacity comparison of $CuAl_2O_4$ and $CuAlFeO_4$ nanospinels with other nanoadsorbent

S.No	Adsorbent	Loading capacity (mg g^{-1})	Reference
1	Fe_3O_4 functionalised with DMSO	116.5	[39]
2	$MnFe_2O_4$@SBA	31.0	[40]
3	Anatase nanoadsorbent	31.2	[41]
4	Fe_2O_3@thiol and Amine	110.1	[42]
5	CuO nanoparticles	97.0	[43]
6	Zn_2GeO_4-EDA nanoribbon	74.6	[44]
7	palygorskite/chitin nanofibers	53.7	[45]
8	CNTs–PAMAM–Ag nanocomposite	18.7	[46]
9	$CuAl_2O_4$ nanospines	163.9	This study
10	$CuAlFeO_4$ nanospines	166.6	This study

3.2.6 Mechanism of adsorption

It is crucial to ascertain the mechanism of adsorption of adsorbate on to the adsorbent and in this study efforts were made to understand how the Pb^{2+} ions are interacting with the $CuAl_2O_4$ and $CuAlFeO_4$ nanospinels. Kinetic experiments and regeneration investigations suggest that the uptake of Pb^{2+} ions by $CuAl_2O_4$ and $CuAlFeO_4$ is physio sorption and electrostatic attraction is dominated as evidenced from pH investigations. The second highly electronegative element oxygen present in the nanospinels will carry negative charge and thus attracts the positively charged Pb^{2+} ion towards them. Further the Alginic acid used during the synthesis process binds onto the nanospinels as a stabilizing agent and the stabilizing agent contains –OH groups which can also involve in the binding of the Pb^{2+} ions. However, the presence of –OH group on nanospinels were not evident in FTIR. Hence, the electrostatic attraction of Pb^{2+} ions by Oxygen atoms should be the dominating factor for the adsorption.

To verify and support the proposed mechanism of adsorption of Pb^{2+} ions by $CuAl_2O_4$ and $CuAlFeO_4$ nanospinels, XPS analysis was carried out. The XPS spectra acquired from the samples reveal the state of surface adsorbed Pb^{2+} ions. The spectra for $CuAl_2O_4$ (pH=6 for 1h) and $CuAlFeO_4$ (pH=6 for 1h) are displayed in Fig.15. The Pb 4f spectrum of the product formed on the surface of adsorbents possesses two broad singlet peaks corresponding to Pb $4f_{7/2}$ and Pb $4f_{5/2}$ centered around binding energy values 138.56 eV and 143.6 eV respectively (Fig. 15a). Based on the NIST XPS database the binding energy values are identified as lead oxy interactions and these values confirms Pb is in +2 oxidation state [47,48]. Similarly the XPS spectra of $CuAlFeO_4$ also displayed two broad singlet peaks corresponding to Pb $4f_{7/2}$ and Pb $4f_{5/2}$ (Fig 15b). These evidence propounds that the Pb^{2+} ions are electrostatically bind onto the $CuAl_2O_4$ and $CuAlFeO_4$ nanospinels and in addition to electrostatic attraction, pore adsorption is also finds a role in the uptake of Pb^{2+} ions.

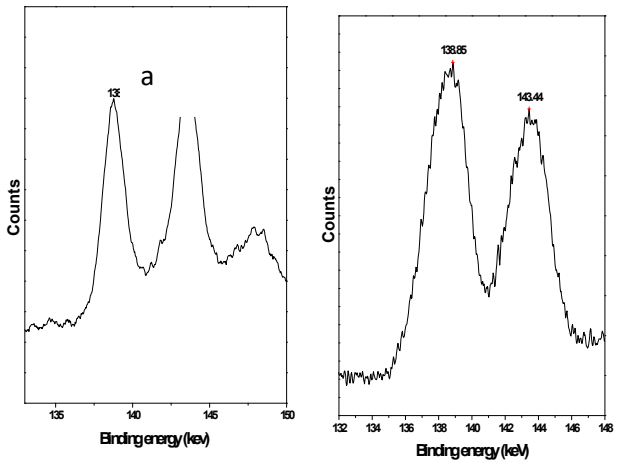

Figure 15. XPS spectra of Pb^{2+} adsorbed a) $CuAl_2O_4$ and b) $CuAlFeO_4$ nanospinels

4 Conclusion

A simple co-precipitation method was employed to synthesize $CuAl_2O_4$ and $CuAlFeO_4$ nanospinels using alginic acid as a polymeric precursor. The formation of the nanospinels was confirmed by XRD, FTIR, SEM, and TEM analyses. The synthesized nanospinels were evaluated as adsorbents for the removal of Pb^{2+} ions from aqueous solutions. A Central Composite Design (CCD) based on Response Surface Methodology (RSM) was developed to optimize the independent variables, namely pH, contact time, and initial Pb^{2+} concentration. The developed models were found to be robust and reliable, with p-values < 0.0001 and predicted and adjusted correlation coefficients close to unity. The three-dimensional surface plots revealed that an optimal pH of 6, along with higher contact times and lower initial Pb^{2+} concentrations, resulted in higher Pb^{2+} removal efficiencies for both $CuAl_2O_4$ and $CuAlFeO_4$ nanospinels. The adsorption studies indicated multilayer adsorption behavior, with each layer of Pb^{2+} adsorption

governed by the Langmuir isotherm. Detailed kinetic investigations showed that the rate-limiting step was not chemisorption, even though the pseudo-second-order model provided the best fit to the kinetic data. The adsorption of Pb^{2+} ions onto $CuAl_2O_4$ and $CuAlFeO_4$ nanospinels was found to be highly spontaneous and exothermic in nature. Furthermore, the nanospinels were successfully regenerated and reused for three adsorption cycles without significant loss of efficiency, demonstrating their economic feasibility and industrial potential. Overall, the results confirm that $CuAl_2O_4$ and $CuAlFeO_4$ nanospinels are efficient adsorbents and hold strong promise for real-time wastewater treatment applications.

Funding statement

This study did not receive any external funding

Conflicts of Interest

Authors declare no conflicts of interest

Data statement

All the required data are provided within the manuscript and in supplemental file.

Author contributions

AG conceptualised and designed the experiments and performed investigations; RL data analysis, manuscript writing, review and design of experiments;

Declarations

Ethical Approval: Not Applicable

Consent to Participate: Not Applicable

Consent to Publish: All authors mutually agree to publish

References

[1] T. Ohgushi and S. Umeno, "Low Temperature Synthesis of Dispersed Fine Particle of Cobalt Aluminate - A New Application of Zeolite, Bull," Chem. Soc. Jpn., vol. 60, no.12, pp. 4457, 1987.

[2] K.T. Jacob, K.P. Jayadevan, R.M. Mallya, Y. Waseda, "Nanocrystalline MgAl2O4: Measurement of Thermodynamic Properties Using a Solid State Cell," Adv. Mater., vol. 12, no. 6, pp. 440-444, 2000.

[3] M. Gaudon, L.C. Robertson, E. Lataste, M. Duttine, M. Ménétrier, A. Demourgues, "Cobalt and nickel aluminate spinels: Blue and cyan pigments," Ceram. Int., vol. 40, no.4, pp. 5201-5207, 2014.

[4] P. Matti, N. Minna, N. Lauri, "Magnesium aluminate thin films by atomic layer deposition from organometallic precursors and water," Thin Solid Films, vol. 466, no. 1-2, pp. 103-107, 2004.

[5] C. Ragupathi, J.J. Vijaya, L.J. Kennedy, M. Bououdina, "Nanostructured copper aluminate spinels: Synthesis, structural, optical, magnetic, and catalytic properties," Mater. Sci. Semicond. Process., 24, pp. 146-156, 2014.

[6] F.L. Dienifer, Horsth, O.P. Julia, D. Mariane, B. Carla, J.A. Fauze, "Colored aluminates pigments obtained from metallic aluminum waste, an opportunity in the circular economy," Clean. Eng. Technol., 5, p. 100313, 2021.

[7] A.M. Bahareh , K. Saeed, T. Sanaz , Y. Amir, "The first catalytic application of copper aluminate nanoparticles in C–C and C–O coupling reaction: green synthesis of some new α - lapachone derivatives," Monatsh. Chem., vol. 147, no. 10, pp. 1849-1854, 2016.

[8] L. Yajie, Q. Shaojun, H. Xiaoning, F. Gang, Z. Rongbin, W. Xiang, W. Shanmin, G. Zhixian and X. Hongwei, "Synthesis and structural characterization of CuAl2O4 spinel with an unusual cation distribution," Journal of Materials and Applications, vol. 7, no.2, pp. 82-89, 2018.

[9] M.K. Satheeshkumar, E.K. Ranjith, C. Srinivas, G. Prasad, S.M. Sher, I. Pradeep, N. Suriyanarayanan, D.L. Sastry, "Structural and magnetic properties of CuFe2O4 ferrite nanoparticles synthesized by cow urine assisted combustion method," J. Magn. Magn. Mater., vol. 484, pp. 120-125, 2019.

[10] L. Li, G. Yu-Meng, Zhang-Hui Lu, Y. Xiaohu, Q. Shaojun, G. Zhixian, Z. Rongbin, F. Gang, "The effects of Fe, Co and Ni doping in CuAl2O4 spinel surface and bulk: A DFT study," Appl. Surf. Sci., vol. 521, p. 146478, 2020.

[11] M. Almokhtar, Atef M. Abdalla, and M. A. Gaffar. "Phase analysis study of copper ferrite aluminates by X-ray diffraction and Mössbauer spectroscopy," J. Magn. Magn. Mater., vol. 272, pp. 2216-2218, 2004.

[12] B.S. Trivedi, N.N. Jani, H.H. Joshi, R.G. Kulkarni, "Cation distribution of the system CuAlxFe2-xO4 by X-rays and Mossbauer studies," J. Mater. Sci., vol. 35, no.21, pp. 5523-5526, 2000.

[13] M. A. Amer, "Spectral studies of the ferrite system Zn(0.5)Cu(0.5)AlxFe2-xO4," HFI, vol. 131, no. 1, pp 29-42, 2000.

[14] S.S. Ata-Allah, M.K. Fayek, Dielectric Relaxation in Mixed Spinel Ferrites Ni1-xCuxAlyFe2-yO4, physica status solidi (a), vol.175, no. 2, pp. 725-733, 1999.

[15] L. Arunkumar, H. Vijayanand, S. Basavaraja, NN. Mallikarjuna, A. Venkataraman, "Lead adsorption

study on combustion derived γ-Fe2O3 surface," Bull. Mater. Sci., vol. 33, no. 1, pp. 1–6, 2010.

[16] Y.C. Sharma, V. Srivastava, S.N. Upadhyay, C.H. Weng, "Alumina Nanoparticles for the Removal of Ni(II) from Aqueous Solutions," Ind. Eng. Chem. Res., vol. 47, no.21, pp. 8095-8100, 2008.

[17] X. Yin, H. Han, M. Kubo, "Adsorption of NH3, NO2 and NO on copper-aluminate catalyst: an ab initio density functional study," Theor Chem Acc., vol. 109, no. 4, pp. 190-194, 2003.

[18] L. Weizhong, L. Bo, Q. Qi, W. Fang, L. Zhongkuan, Z. Peixin, W. Shaohui, "Synthesis, characterization and photocatalytic properties of spinel CuAl2O4 nanoparticles by a sonochemical method," J. Alloys Compd., vol. 479, no. 1-2, pp. 480-483, 2009.

[19] J. Yanyan, L. Jinggang, S. Xiaotao, "CuAl2O4 powder synthesis by sol-gel method and its photodegradation property under visible light irradiation," J Sol-Gel Sci Technol., vol. 42, no.1, pp. 41-45, 2007.

[20] M. Kebir, M. Chabani, N. Nasrallah, A. Bensmaili, M. Trari, "Coupling adsorption with photocatalysis process for the Cr(VI) removal," Desalination, vol. 270, no. 1-3, pp. 166-173, 2011.

[21] M.J. Iqbal and S. Farooq, "Effect of doping of divalent and trivalent metal ions on the structural and electrical properties of magnesium aluminate," Mater. Sci. Eng., B, vol. 136, no. 2-3, pp. 140-147, 2007.

[22] N.V. Vegten, T. Baidya, F. Krumeich, W. Kleist, A. Baiker, "Flame-made MgAl2−xMxO4 (M= Mn, Fe, Co) mixed oxides: Structural properties and catalytic behavior in methane combustion," Appl. Catal., B., vol. 97, no. 3-4, pp.398-406, 2010.

[23] M.J. Iqbal and B. Ismail, "Electric, dielectric and magnetic Characteristics of Cr3+, Mn3+ and Fe3+ substituted MgAl2O4: Effect of pH and annealing temperature," J. Alloys Compd., vol. 472, no.1-2, pp. 434-440, 2009.

[24] T.P. Yadav, N.K. Mukhopadhyay, R.S. Tiwari, O.N. Srivastava, "Synthesis of nanocrystalline (Co, Ni)Al2O4 spinel powder by mechanical milling of quasicrystalline material," J. Nanosci. Nanotechnol., vol. 7, no.2, pp. 575-579, 2007.

[25] V. Radhika, S. Subramanian, K.A. Natarajan, "Bioremediation of Zinc using desulfotomaculum nigrificans: bioprecipitation and characterization studies," Water Res., vol. 40, no.19, pp. 3628-3636, 2006.

[26] C. Quintelas, Z. Rocha, B. Silva, B. Fronseca, H. Figueiredo, T. Taveras, "Removal of Cd(II), Cr(IV), Fe(III) and Ni(II) from aqueous solutions by an E.coli biofilm supported on kaolin," Chem.Eng.J., vol. 149, no. 1-3, pp. 319-324, 2009.

[27] J. Goel, K. Kadirvelu, C. Rajagopal, V.K. Garg, "Removal of lead (II) from aqueous solution by adsorption on carbon aerogel using a response surface methodological approach," Ind.Eng. Chem. Res., vol. 44, no.7, pp. 1987-94, 2005.

[28] V Andal, G. Buvaneswari, R. Lakshmipathy, "Synthesis of CuAl2O4 Nanoparticle and Its Conversion to CuO Nanorods," J. Nanomater. Vol. 2021, no.1, p. 8082522, 2021.

[29] G. Yiming, F. Huixia, W. Bin, Q. Jianhui, M. Xuefen, Z. Liang, Z. Bin, C. Nali, T. Lin, "Adsorption of Pb2+ by inorganic liquid-treated sepiolite: Adsorption process optimization and mechanism analysis via response surface methodology," Microporous Mesoporous Mater., vol. 363, p. 112821, 2024.

[30] S. Tasrin, S. Vivek, S. Senthilmurugan, N. Selvaraju, "Multivariate optimisation of Cr (VI), Co (III) and Cu (II) adsorption onto nanobentonite incorporated nanocellulose/chitosan aerogel using response surface methodology," J. Water Process Eng., vol. 36, p. 101283, 2020.

[31] F. Sabbagh, I.I. Muhamad, Z. Nazari, P. Mobini, S.B. Taraghdari, "From formulation of acrylamide-based hydrogels to their optimization for drug release using response surface methodology," Mater. Sci. Eng. C., 92, pp. 20-25, 2018.

[32] K. Pyrzynska, Preconcentration and removal of Pb (II) ions from aqueous solutions using graphene-based nanomaterials. Materials, vol. 16(3), pp. 1078, 2023.

[33] R. Jayachandra, R. Lakshmipathy, S.R. Rajasekhara, "Hydrophobic D-galactose based ionic liquid for the sequestration of Pb2+ ions from aqueous solution," J. Mol. Liq., vol. 219, pp. 1172-1178, 2016.

[34] J.I. Prince, A. Sivakumar, MSM. Kamil, K.K. Cheralathan, R. Lakshmipathy, "Synthesis of zeolite/activated carbon composite material for the removal of lead (II) and cadmium (II) ions," Environmental Progress and Sustainable Energy, vol. 38, no. 6, p.e13246, 2019.

[35] W. Chen, Z. Lu, B. Xiao, P. Gu, W. Yao, J. Xing, et al., Enhanced removal of lead ions from aqueous solution by iron oxide nanomaterials with cobalt and nickel doping. Journal of Cleaner Production, Vol.211, pp. 1250-1258, 2019.

[36] C. Mingcan, J. Min, C. Sang - Hyun, K. Jeehyeong, "Kinetic and thermodynamic studies of the adsorption of heavy metals on to a new adsorbent: coal mine drainage sludge," Environ. Technol., vol. 31, no. 11, pp. 1203-1211, 2010.

[37] A. Wang, Y. Chu, T. Muhmood, "Adsorption properties of Pb2+ by amino group's functionalized montmorillonite from aqueous solutions," J. Chem. Eng. Data., vol. 63, no.8, pp. 2940-2949, 2018.

[38] S. Chakravarty, M. Ashok, T.N. Sudha, A.K. Upadhyay, J. Kona, J.K. Sircar, A. Madhukar, K. K. Gupta, "Removal of Pb(II) ions from aqueous solution by adsorption using bael leaves (Aegle marmelos)," J. Hazard. Mater., vol. 173, no. 1–3, pp. 502-509, 2010.

[39] V.P. Kothavale, A. Sharma, R.P. Dhavale, V.D. Chavan, S.R. Shingte, O. Selyshchev, T.D. Dongale, H.H. Park, D.R.T. Zahn, G. Salvan, P.B. Patil, "Carboxyl and thiol-functionalized magnetic nanoadsorbents for efficient and simultaneous removal of Pb(II), Cd(II), and Ni(II) heavy metal ions from aqueous solutions: Studies of adsorption, kinetics, and isotherms," J. Phys. Chem. Solids., vol. 172, p. 111089, 2023.

[40] B.L. Feysal, H.S.M.S. Reza, M. Mahsasadat, A.P. Homayon, M. Elham, "Highly efficient removal of toxic As(V), Cd (II), and Pb(II) ions from water samples using MnFe2O4@SBA-15-(CH2)3-adenine as a recyclable bio-nanoadsorbent," Microporous Mesoporous Mat., vol. 356, p. 112567, 2023.

[41] O.K. Züleyha, Y. Yuda, "Synthesis and characterization of anatase nanoadsorbent and application in removal of lead, copper and arsenic from water," Chem. Eng. J., vol. 225, pp. 625-635, 2013.

[42] J. Jiujiang, C. Guo, Z. Jun, "Preparation and characterization of amino/thiol bifunctionalized magnetic nanoadsorbent and its application in rapid removal of Pb (II) from aqueous system," J. Hazard. Mater., vol. 368, pp. 255-263, 2019.

[43] Z. Rumman, U.K. Saif, A. Ameer and H.F. Izharul, "A study on effective adsorption of lead from an aqueous solution using Copper Oxide nanoparticles," IOP Conf. Ser.: Mater. Sci. Eng., vol. 1058, no.1, p. 012074, 2021.

[44] L. Yu, R.J. Zou, Z.Y. Zhang, G.S. Song, Z.G. Chen, J.M. Yang, J.Q. Hu, "A Zn2GeO4–ethylenediamine hybrid nanoribbon membrane as a recyclable adsorbent for the highly efficient removal of heavy metals from contaminated water," Chem. Commun., vol. 47, no. 38, pp. 10719-10721, 2011.

[45] C.M. Stanley, S.G. Pei, F.I. Ahmad, A.M.A. Mohamed, A.A. Nor, D.S. Nur, O.R. Yusuf, "Facile preparation of palygorskite/chitin nanofibers hybrids nanomaterial with remarkable adsorption capacity," Mater. Sci. Eng. B., vol. 262, p. 114725, 2020.

[46] G.M. Neelgund, S.F. Aguilar, M.D. Kurkuri, D.F. Rodrigues, R.L. Ray, "Elevated Adsorption of Lead and Arsenic over Silver Nanoparticles Deposited on Poly(amidoamine) Grafted Carbon Nanotubes," Nanomaterials vol. 12, no.21, p. 3852, 2022.

[47] Swiatkowski, Andrzej, et al. "Influence of the surface chemistry of modified activated carbon on its electrochemical behaviour in the presence of lead (II) ions." Carbon., vol. 42, no. 15, pp. 3057-3069, 2004.

[48] S. Yang, W. Su, S.D. Lin, J. Rick, J. Cheng, J. Liu, C. Pan, D. Liu, J. Lee, T. Chan, H. Sheu and B. Hwang, "Preparation of nano-sized Cu from a rod-like CuFe2O4: Suitable for high performance catalytic applications," Appl. Catal., B., vol. 106, no. 3-4, pp. 650-656, 2011.